Available online at www.sciencedirect.com
SCIENCE DIRECT
Journal of Theoretical Biology 241 (2006) 601–616
Journal of Theoretical Biology
www.elsevier.com/locate/yjtbi

Potential role of natural enemies during tree range expansions following climate change

P.R. Moorcroft[a,*], S.W. Pacala[b], M.A. Lewis[c,d]

[a]OEB Department, Harvard University, 22 Divinity Ave Cambridge, MA 02138, USA
[b]Department of Ecology and Evolutionary Biology, Princeton University, Princeton, NJ 08544-1003, USA
[c]Department of Mathematical & Statistical Sciences, University of Alberta, 545B Central Academic Building Edmonton Alberta, Canada T6G 2G1
[d]Department of Biological Sciences, University of Alberta, 545B Central Academic Building Edmonton Alberta, Canada T6G 2G1

Received 2 March 2005; received in revised form 23 December 2005; accepted 27 December 2005
Available online 24 February 2006

Abstract

Recent investigations have shown how chance, long-range dispersal events can allow tree populations to migrate rapidly in response to changes in climate. However, this apparent solution to *Reid's paradox* applies solely within the context of single species models, while the rapid migration rates seen in pollen records occurred within multispecies communities. Ecologists are therefore presented with a new challenge: reconciling the macroscopic dynamics of spread seen in the pollen record with the rules and interactions governing plant community assembly. A case that highlights this issue is the rapid spread of Beech during the Holocene into a landscape already dominated by a close competitor, Hemlock. In this study, we analyse a simple model of plant community assembly incorporating competition for space and dispersal dynamics, showing how, even when a species is capable of rapid migration into an empty landscape, the presence of an ecologically similar competitor causes Reid's paradox to re-emerge because of the dramatic slowing effect of competitive interactions on a species' rate of spread. We then show how the answer to the question of how tree species dispersed rapidly into occupied landscapes may lie in secondary interactions with host-specific pathogens and parasites. Inclusion of host-specific pathogens into the simple community assembly model illustrates how tree species undergoing range expansions can temporarily outstrip specialist predators, giving rise to a transient Jansen–Connell effect, in which the invader acts as temporary 'super-species' that spreads rapidly into communities already occupied by competitors at rates consistent with those observed in the paleo-record.

Keywords: Tree migration; Long-distance dispersal; Pathogens; Transient Janzen–Connell effects; Tree range expansions

1. Introduction

An important measure of our ability to predict the response of tree species future to changes in climate is our ability to understand their dynamics in response to past climate change (Delacourt and Delacourt, 1987; Huntley et al., 1991; Overpeck et al., 1991; Webb et al., 1998). Palynological studies indicate that the retreat of the Laurentide ice-sheet during the Holocene was accompanied by a large-scale reorganization in the geographic distribution of tree species across the North American continent (Davis, 1976; Delacourt and Delacourt, 1987; Webb, 1987; Huntley et al., 1988). The rates at which tree species spread during this period appear to have been surprisingly rapid, in some cases in excess of a hundred meters per year (Delacourt and Delacourt, 1987; Clark, 1993).

The discrepancy between the rapid rates of spread seen in the palynological record and the measured dispersal distances of trees in ecological studies has been a long-standing issue in plant biogeography. Recently, this has become known as *Reid's paradox*, in honor of the pioneering observations by Reid (1899) who found that the spread of Oaks into Great Britain at the end of the Pleistocene were seemingly impossibly fast (Clark et al., 1998).

In seeking to reconcile the rapid spread of trees in response to changes in past climate with the measured

*Corresponding author. Tel.: +1 617 496 6744; fax: +1 617 495 9484.
E-mail addresses: pmoorcroft@oeb.harvard.edu, paul_moorcroft@harvard.edu (P.R. Moorcroft).

0022-5193/$ - see front matter © 2006 Elsevier Ltd. All rights reserved.
doi:10.1016/j.jtbi.2005.12.019

dispersal distances of tree species, researchers have developed a variety of models of plant dispersal dynamics. Early models (e.g. Skellam, 1951) used diffusion-terms within deterministic equations to describe the spatial spread of tree populations, reflecting an underlying assumption of a Gaussian spatial distribution of seedlings around parent trees. However, these models were later shown to have difficulty in accounting for the rapid rates of spread seen in tree pollen data (Clark et al., 1998). Subsequent researchers considered more realistic models of dispersal that included stochasticity in plant demographic rates, and, most importantly, the possibility of chance, long-range dispersal, giving rise to leptokurtic, 'fat-tailed' rather than Gaussian dispersal kernels (Kot et al., 1996; Clark, 1998; Higgins and Richardson, 1999; Lewis and Pacala, 2000). These analyses showed that, when incorporated into single-species models of plant dispersal, 'fat-tailed' distributions can result in rates of spread consistent with those observed in the palynological record (Clark, 1998, 2003).

This apparent reconciliation of the macroscopic rates of spread seen in the paleo-record with the dispersal and demographic properties of trees has, however, been solely within the context of models for the dynamics of single species, while the rates of spread inferred from pollen data occurred in multi-species communities. For example, Fig. 1 shows the changes in the spatial distribution of Hemlock (*Tsuga canadensis*) and Beech (*Fagus grandifolia*) during the Holocene inferred from analyses of fossil pollen data (North American Pollen Database Contributors, 2005). The figure indicates a northward expansion of Hemlock followed by a subsequent migration of Beech into the areas occupied by Hemlock.

Hemlock's advance ahead of Beech is most likely explained by its ability to tolerate lower precipitation (Kessel, 1979; Caspersen et al., 1999; Caspersen and Kobe, 2001), but in most all other aspects, these two species are very similar ecologically, occupying the same shade-tolerant, late-successional niche within north–eastern forests of the United States. Field measurements of growth, mortality and recruitment rates (Canham, 1985; Pacala et al., 1996) confirm the remarkable closeness in their life-history strategies (Fig. 2), and simulations using

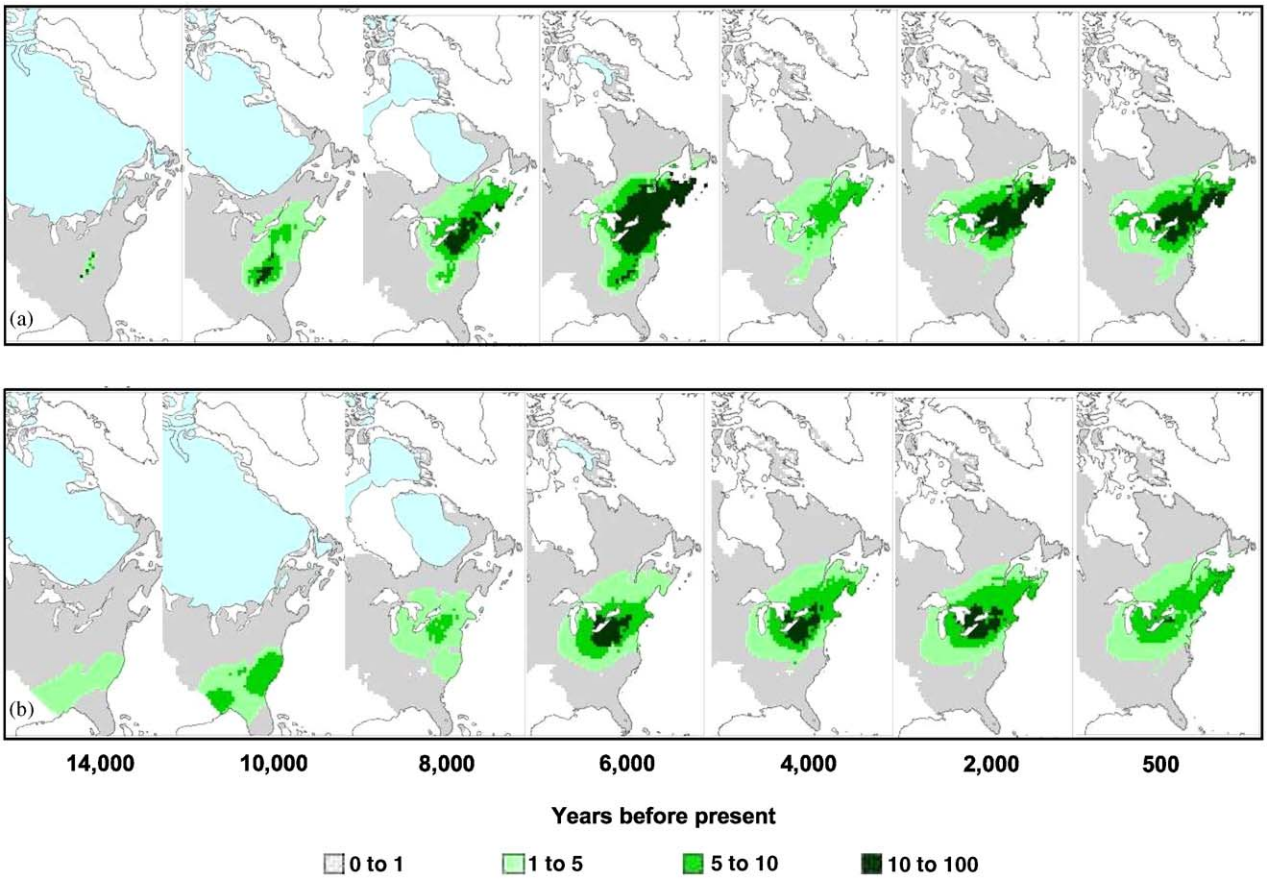

Fig. 1. Spatial spread of (a) Hemlock (*Tusga canadensis*) and (b) Beech (*Fagus grandifolia*) following the retreat of the Laurentide Ice sheet during the Holocene inferred from the 2005 North American Pollen Database (North American Pollen Database Contributors, 2005). Light-blue indicates the position of the ice-sheet while the grey to green colors indicate relative frequency of pollen in different areas. Images generated using Pollen Viewer v.3.2 (Brown University Quaternary Environment Group and Bartlein, 2005). Note the rapid expansion of Beech following the decline in Hemlock that occurred at 4000 BP. Decline rate of spread in (b) is similar to Hemlock's rate of spread in (a), despite the prior colonization by its close competitor, Hemlock.

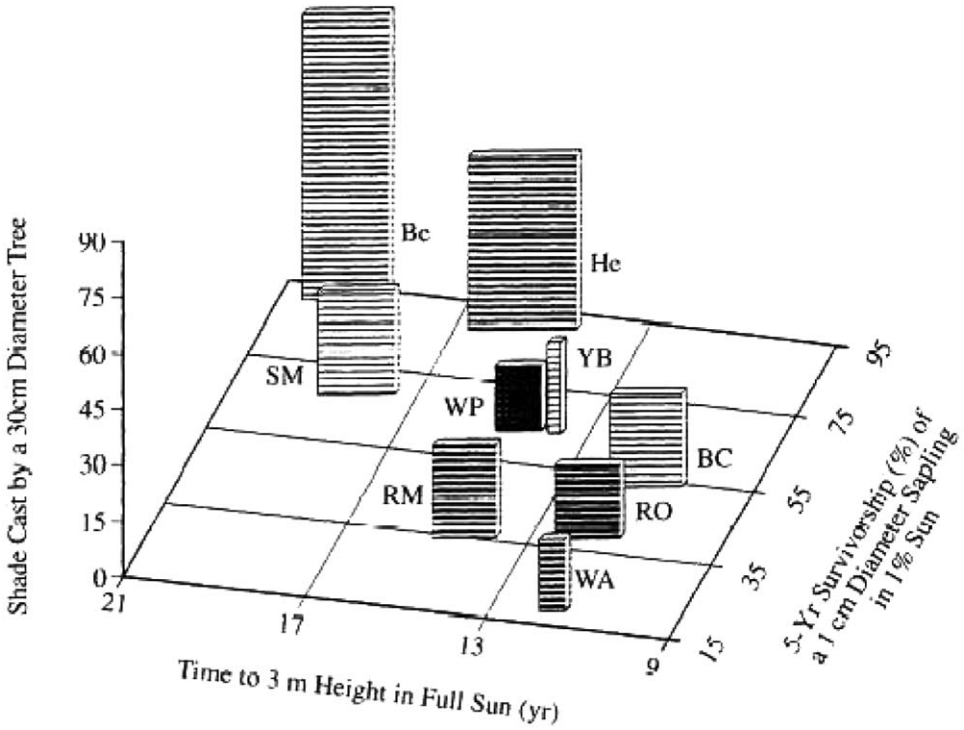

Fig. 2. Ecological similarity in the niches of Hemlock and Beech. Plots shows the position of Hemlock and Beech and other major New-England tree species in a three-dimensional space consisting of the following key measures of plant performance: survivorship of a 1 cm diameter sapling in 1% full sun, the number of years it takes a seedling to reach 3 m in full sun, and the amount of shade cast by a 30 cm adult tree. Two-letter codes reflect the common names of the tree species (Be = Beech, He = Hemlock, SM = Sugar Maple, RM = Red Maple, WP = White Pine, YB = Yellow Birch, RO = Red Oak, BC = Black Cherry, WA = White Ash). From Pacala et al. (1996).

empirically-calibrated individual-based models of forest dynamics have shown that this translates into almost identical competitive abilities under most conditions (Pacala et al., 1996). A characteristic signature of their niche similarity that emerges in simulations is the formation and long-term persistence of endogenously-generated patchiness in the spatial distributions of the two species—a phenomenon that is borne out empirically (Davis et al., 1992; Frelich et al., 1993; Davis et al., 1994).

As shown previously using a spatial version of the Lotka–Volterra phenomenological model of competition (Okubo et al., 1989; Shigesada and Kawasaki, 1997), and here using a mechanistic model of plant community assembly, whenever a colonizing species disperses into a landscape in which an ecologically similar species is present, we expect a marked slowing in the colonizer's rate of spread. In light of this, what is remarkable in Fig. 1 is that the presence of Hemlock (Fig. 1a) does not appear to have significantly slowed the subsequent northward expansion of Beech (Fig. 1b). Given the presence of its close ecological competitor, Hemlock, Beech's rate of spread is surprisingly rapid—in excess of a hundred meters per year (Woods and Davis, 1989).

We then use our plant community assembly model to explore an idea first proposed by Davis (1981) that interactions with pathogens and parasites may have played a role in facilitating the rapid rates of tree spread in response to climate change. The essence of the idea is as follows: trees are susceptible to a variety of pathogens that are host-specific either at the level of species, genus or family. During periods of colonization, species may be able to outstrip their host-specific pathogens, and this escape from parasitism will facilitate their rate of spread by giving them a competitive advantage over ecologically similar resident species. More recently, a similar explanation has been proposed for the spread of invasive species (Keane and Crawley, 2002; Mitchell and Power, 2003).

While numerous models have been developed to explore the spatial spread of predators and pathogens (see Shigesada and Kawasaki, 1997 for a review, and also Owen and Lewis, 2001), these models have focused exclusively on the dynamics of the predator–prey or pathogen–host interaction. Here, we develop a model to analyse how interactions with host-specific pathogens affect the dynamics of competition between a colonizing tree species and an ecologically similar resident. Our analysis reveals how the interactions of the colonizer and resident with their respective pathogens can have a profound impact on the dynamics of competition, the rate of colonizer spread, and the resulting dynamics of community re-assembly (cf. Hilker et al., 2005).

2. Analysis

2.1. Colonization dynamics of competitively similar species

Suppose a plant community consists of two ecologically similar plant species that compete for space, and the rate at which they colonize empty sites[1] is governed by the rate at which their offspring disperse in from other areas (Fig. 3). This model can be written mathematically as

$$\frac{\partial S_1}{\partial t}(x,t) = \underbrace{U(x,t) f_1 \int_\Omega D_1(y-x) S_1(y,t)\,\mathrm{d}y}_{recruitment} - \underbrace{\mu_1 S_1(x,t)}_{mortality}, \quad (1)$$

$$\frac{\partial S_2}{\partial t}(x,t) = \underbrace{U(x,t) f_2 \int_\Omega D_2(y-x) S_2(y,t)\,\mathrm{d}y}_{recruitment} - \underbrace{\mu_2 S_2(x,t)}_{mortality}, \quad (2)$$

where $S_1(x,t)$ and $S_2(x,t)$ are densities of species 1 and 2 at location x, and $U(x,t) = K - S_1(x,t) - S_2(x,t)$, is the density of unoccupied sites at position x within the region Ω. $D_1(x)$ and $D_2(x)$ are the dispersal kernels of the two species; f_1 and f_2 are their fecundities; and μ_1 and μ_2 are their mortality rates.

The above equations can be simplified by introducing the following non-dimensionalized variables:

$$S_1^* = \frac{S_1}{K}, \quad S_2^* = \frac{S_2}{K},$$
$$t^* = t\mu_1, \quad \mu_2^* = \frac{\mu_2}{\mu_1}, \quad x^* = \frac{x}{L},$$
$$f_1^* = \frac{f_1 K}{\mu_1}, \quad f_2^* = \frac{f_2 K}{\mu_1}, \quad (3)$$

where L is characteristic length-scale from either D_1 or D_2. Inserting the above definitions into Eqs. (2)–(13), and then dropping the asterisks yields:

$$\frac{\partial S_1}{\partial t}(x,t) = (1 - S_1(x,t) - S_2(x,t)) f_1 \int_\Omega D_1(y-x) \times S_1(y,t)\,\mathrm{d}y - S_1(x,t), \quad (4)$$

$$\frac{\partial S_2}{\partial t}(x,t) = (1 - S_2(x,t) - S_2(x,t)) f_2 \int_\Omega D_2(y-x) \times S_2(y,t)\,\mathrm{d}y - \mu_2 S_2(x,t), \quad (5)$$

$S_1(x,t)$ and $S_2(x,t)$ are now the proportion of sites occupied by species 1 and 2.

2.1.1. Colonization dynamics

We begin by examining the colonization dynamics predicted by Eqs. (4)–(5), considering the arrival of the second species at the edge of a one-dimensional monoculture of the first species at equilibrium. The model's parameter values are set to reflect the general characteristics of forest communities: reflecting the closed-canopy nature of forest landscapes, we set fecundity high relative to mortality rates (i.e. $f_1, f_2 \gg 1$), resulting in high levels of site occupancy; and following the extensive work by Neubert et al. (1995), Kot et al. (1996), Lewis and Pacala (2000) and Clark (1998), the dispersal kernels $D_1(x)$ and $D_2(x)$ are assumed to be comprised of a joint Laplace kernel with a short-range and a long-range dispersal component ($D(x) = (1-p)\exp(-|x|)/2 + p\exp(-\beta_l|x|)/2$, where $1/\beta_l$ is the average long-range dispersal distance relative to the average short-range dispersal distance component, and p determines the fraction of reproduction that goes into long dispersal). For simplicity, we also assume that the mortality rates and dispersal kernels of the two species are identical ($\mu_1, \mu_2 = 1$ and $D_1 = D_2$). See Table 1 for details of the parameter values used in this analysis.

Figs. 4 and 5 show the effect of the presence of a resident species on the rate of spread of a colonizer that has a 50%

[1]Defined as canopy gap-sized areas approximately the size of adult canopy tree.

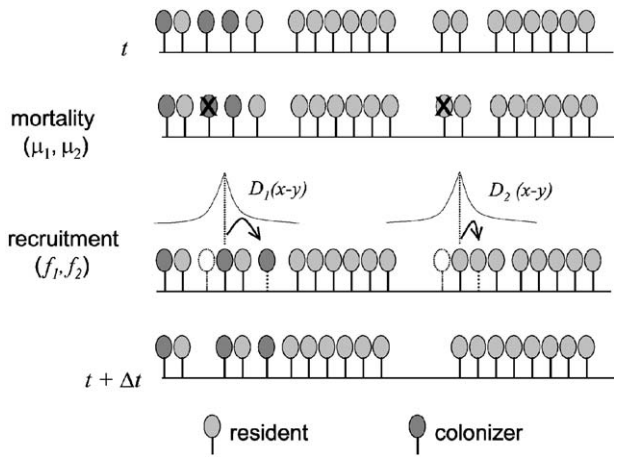

Fig. 3. Schematic illustrating the community assembly model formulation (Eqs. (4)–(5)). The model formulation describes the mortality and recruitment dynamics of two tree species occupying a one-dimensional landscape, which compete for unoccupied sites (gap-sized areas approximately the size of a single adult tree). As the figure illustrates, the model is used to explore the colonization dynamics that occur when one of species (dark grey ovals) arrives at a edge of the landscape that is occupied by the other species at its single species equilibrium (light grey ovals).

Table 1
Initial parameter values used in the community assembly model Eqs. (1)–(2)

Parameter	Quantity	Value
μ_2	Mortality rate of species 2 relative to species 1	1
f_1	Fecundity of species 1	100
f_2	Fecundity of species 2	150
$1/\beta_l$	Average long dispersal distance relative short dispersal distance	10
p	Fraction of fecundity going to long dispersal	0.1

All quantities are dimensionless (see Eq. 3).

higher rate of seed production, but in all other respects is identical to the resident. In the absence of the resident, the colonizing species moves rapidly into the community (Fig. 4). Assuming canopy trees have ~50-year lifespan and that the mean dispersal distance of the tree's short dispersal kernel ~10 m (i.e. $\mu_1 = 0.02\,\mathrm{yr}^{-1}$, and $1/\beta_s = 10\,\mathrm{m}$), the colonizer's rate of spread is ~200 m/yr, a speed that is consistent with the findings of earlier studies using single-species models.

However, in the presence of the ecologically similar resident, the colonizer's rate of spread is reduced to under 2 m/yr (Fig. 5). Thus, despite a significant fecundity advantage over the resident, the low availability of vacant sites within the community means that the colonizer's rate of spread is two-orders of magnitude lower due to presence of the other species (Fig. 5).

By linearizing the equation describing the dynamics of the colonizing species (Eq. (5)) about its leading edge (see Appendix A), we can obtain the following analytic expression for how the colonist's asymptotic rate of spread c^*, varies as a function of the fecundity, mortality and dispersal characteristics of the colonizer and resident:

$$c^* = \min_{a>0} \frac{1}{a}(f_2(1-\bar{S}_1)\hat{D}(a) - \mu_2), \tag{6}$$

where $\bar{S}_1 = 1 - (1/f_1)$ is the equilibrium density of species 1 in the absence of species 2, and $\hat{D}(a)$ is the moment generating function of the dispersal kernel.

Fig. 6 shows how c^* changes as a function of the relative fecundity of the colonizer. For the simulation shown in Fig. 5, Eq. (A7) is positive, indicating that colonizer spreads into the community. However, the rate of spread is only 1.8 m/yr, well below the rate at which it colonizes empty habitat (dotted line), and well below the typical values seen in the paleo-record (shaded area). As the fecundity advantage of the colonizer over the resident increases its rate of spread increases, but not substantially; even when the fecundity of the colonizer is twice that of the resident, the rate of colonization is still only 3.4 m/yr. Conversely, as the colonizer's advantage declines and it becomes more similar to the resident, its rate of colonization slows until, when the species are identical, its rate of colonization is zero (Fig. 6). Analysis shows that in this situation, a 'neutral invasion' occurs in which the colonizing species never increases in abundance and the initial pulse of colonists simply mixes into the community (Appendix A.1).

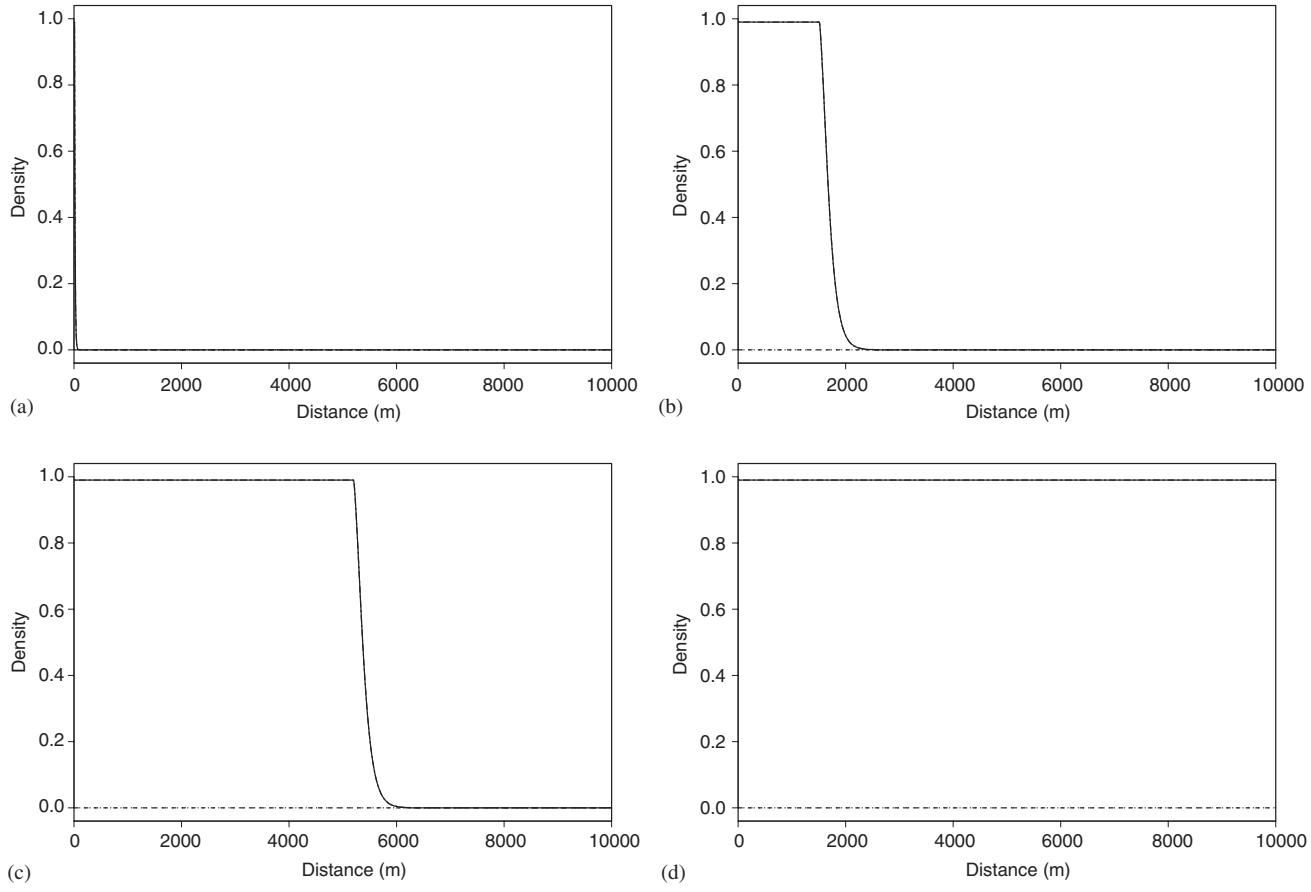

Fig. 4. Dynamics of a colonizing species dispersing onto an empty landscape. Panels (a)–(d) show the spatial distribution of the colonizer (−) at different times t (years) following its arrival at the edge of a one-dimensional domain. To aid interpretation, the non-dimensionalized rate of spread obtained from the solution of Eqs. (4)–(5) has been converted into dimensional units of meters per year (see text for details). (a) $t = 0$ yr, (b) $t = 100$ yr, (c) $t = 250$ yr and (d) $t = 500$ yr. Spatial position is indicated by the distance (m) from the left edge of the domain.

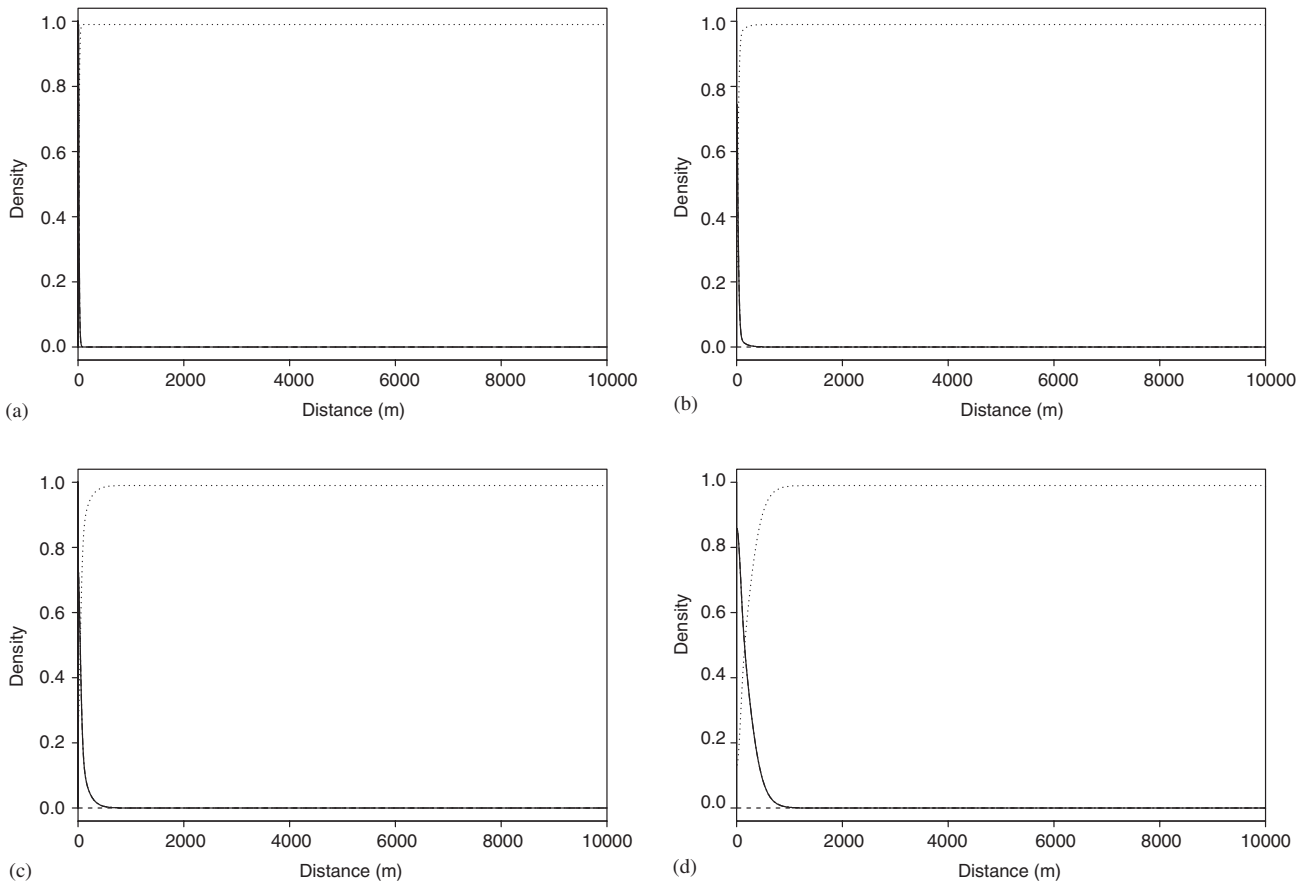

Fig. 5. Colonization dynamics of a competitively similar species in the absence of pathogens. Panels (a)–(d) show the spatial distribution of the resident (···) and colonizer (−) at different times t (years) following the arrival of the colonizing species at the edge of a one-dimensional community of the resident species at equilibrium. (a) $t = 0$ yr, (b) $t = 100$ yr, (c) $t = 250$ yr and (d) $t = 500$ yr. Spatial position is indicated by the distance (m) from the left edge of the domain.

2.2. Effect of host-specific pathogens on colonization dynamics

We now extend Eqs. (4)–(5) to consider the effect of host-specific pathogens on the above colonization dynamics (Fig. 7). Suppose that individuals of both species are susceptible to infection by dispersing host-specific pathogens that reduce the fecundity of infected individuals but do not infect their offspring. Including a simple representation of this process into Eqs. (4)–(5) yields the following non-dimensionalized equations for the dynamics of the trees and their pathogens:

$$\begin{aligned}\frac{\partial S_k}{\partial t}(x,t) &= \underbrace{U(x,t) f_k \int_\Omega D(y-x)[S_k(y,t)+\delta I_k(y,t)]\,\mathrm{d}y}_{\textit{recruitment}} \\ &\quad - \underbrace{R_0^{(k)} S_k(x,t) \int_\Omega B_k(y-x) I_k(y,t)\,\mathrm{d}y}_{\textit{infection}} \\ &\quad - \underbrace{\mu_k S_k(x,t)}_{\textit{mortality}}, \end{aligned} \tag{7}$$

$$\begin{aligned}\frac{\partial I_k}{\partial t}(x,t) &= \underbrace{R_0^{(k)} S_k(x,t) \int_\Omega B_k(y-x) I_k(y,t)\,\mathrm{d}y}_{\textit{infection}} \\ &\quad - \underbrace{\mu_k I_k(x,t)}_{\textit{mortality}} \quad (k=1,2), \end{aligned} \tag{8}$$

where $S_k(x,t)$ and $I_k(x,t)$ are the proportion of sites occupied by uninfected and infected individuals of species k, $U(x,t)$ is the density of unoccupied sites, δ_k is the fecundity of infected individuals relative to uninfected individuals, $R_0^{(k)}$ is non-dimensionalized intrinsic reproductive rate of species k's host-specific pathogen ($R^{(k)*} = R^{(k)}K/\mu_1$). $B_k(x)$ is the non-dimensionalized dispersal kernel of species k's host-specific pathogen, and $\mu_1 = 1$. The remaining parameters are the same as in Eqs. (4)–(5), except that the fraction of unoccupied sites $U(x)$ is now given by $1 - S_1(x,t) - I_1(x,t) - S_2(x,t) - I_2(x,t)$.

We begin by considering the case where the intrinsic reproductive rates of both species' pathogens $R_0^{(1)}$ and $R_0^{(2)}$ are identical, and that the spatial distribution of pathogen infection $B_k(x)$ matches that of their hosts (Table 2).

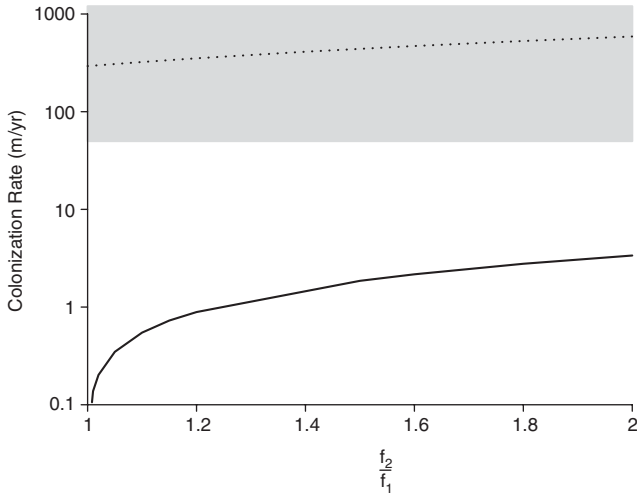

Fig. 6. Colonization rate in the absence of host-specific pathogens (solid line) as function of the relative fecundity of the colonizing species. Plot shows the asymptotic rate of colonization c^* in m/yr as a function of f_2/f_1, the fecundity of the colonizer relative to that of the resident. Shaded area indicates the typical rates of spread observed in the paleo-record (Delacourt and Delacourt, 1987; Clark, 1998). Solid line shows c^* for the dynamics in the absence of pathogens (Eq. (A7)). When colonizers have a fecundity advantage over the resident ($f_2/f_1 > 1$), the colonizer moves into the community with a positive characteristic asymptotic speed $c^* > 0$, but the rate of movement remains far below the typical rates observed in the paleo-record. When the species are identical ($f_2/f_1 = 1$), $c^* = 0$ and a neutral invasion occurs (see Appendix A.1). Dotted line shows colonizer's rate of movement into empty habitat (Eq. (A8)).

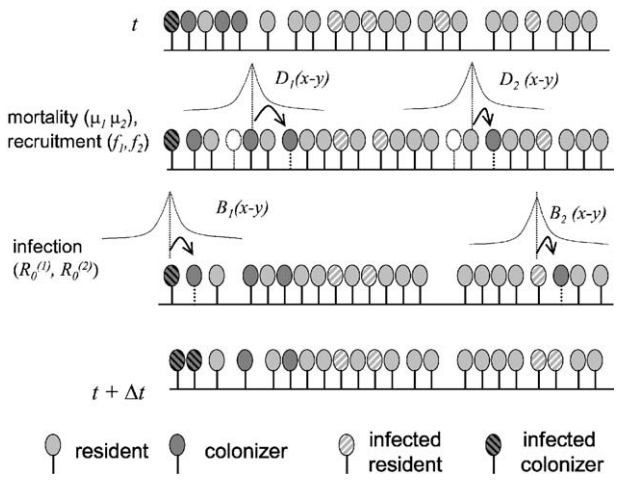

Fig. 7. Schematic illustrating the community assembly model incorporating host-specific pathogen dynamics (Eqs. (7)–(8)). In addition to the growth, mortality, and recruitment dynamics of the two tree species shown in Fig. 3, healthy individuals of each species j ($j = 1, 2$), are susceptible to infection by a host-specific pathogen with intrinsic reproductive rate of $R_0^{(j)}$ and dispersal kernel $B_j(x)$. Infection reduces fertility of infected individuals to a function δ of uninfected individuals. The model is used to explore the colonization dynamics that occurring the presence of host-specific pathogens when the second species (dark grey ovals) arrives at a edge of the landscape that is occupied by the first species at its single species equilibrium (light grey ovals). Hatching indicates infected individuals of each species.

Table 2
Table of pathogen parameters used in the initial simulation of community assembly model incorporating interactions with host-specific pathogens (Eqs. (7)–(8)) shown in Fig. 8

Parameter	Quantity	Value
R_0	Intrinsic reproductive rate of pathogen	0.5
δ	Fecundity of infected plants relative to disease-free plants	0
q	Proportion of R_0 going to long dispersal	0.1
γ_s	Pathogen's average short dispersal distance Relative to tree species 1's short range dispersal distance	1
γ_l	Pathogen's average long dispersal distance Relative to tree species 1's short range dispersal distance	10

All quantities are dimensionless (see Eq. 15).

2.2.1. *Colonization dynamics in the presence of host-specific pathogens*

As in Section 2.1, we consider the introduction of the second species to the edge of a resident equilibrium community of the other species, but this time in conjunction with its host-specific pathogen. The colonization dynamics that now occur are markedly different. Fig. 8 shows the dynamics of spread when the plants have the same properties as in Fig. 5, with host-specific pathogens whose dispersal abilities match that of their hosts, and that reduce the fecundity of infected individuals to zero (see Table 2).

Following their introduction, individuals of the colonizing species escape from their pathogens at the edge of their distribution (Figs. 8a,b). This then begins to facilitate the colonizer's spread into the resident community, and the colonizing population quickly organizes into a pair of lagged waves: a wave of uninfected plants, followed by a wave of infected individuals some distance behind (Fig. 8c). Ahead of their pathogens, uninfected individuals of the colonizing species are able to out-compete the resident population whose density is depressed due its host-specific pathogen, enabling the colonizer to spread rapidly and reach high levels of abundance (Figs. 8d–e). The plant community eventually arrives at a new equilibrium that is comprised of a mixture of the two species (Fig. 8f). The net effect of the interaction with pathogens is to sweep the second species rapidly into the community at a rate far faster than when interactions with host-specific pathogens are absent (compare Figs. 5 and 8).

Using similar approaches to the one employed in Section 2.1, we can gain analytic insight into these colonization dynamics. Analysis (Appendix B) indicates that the colonization rate c^* is determined by the rate at which uninfected colonizers are able to spread into the infected resident community of the other species. The speed of this process is given by

$$c^* = \min_{a>0} \frac{1}{a}\left(f_2(1 - \bar{S}_1 - \bar{I}_1)\hat{D}(a) - \mu_2\right), \tag{9}$$

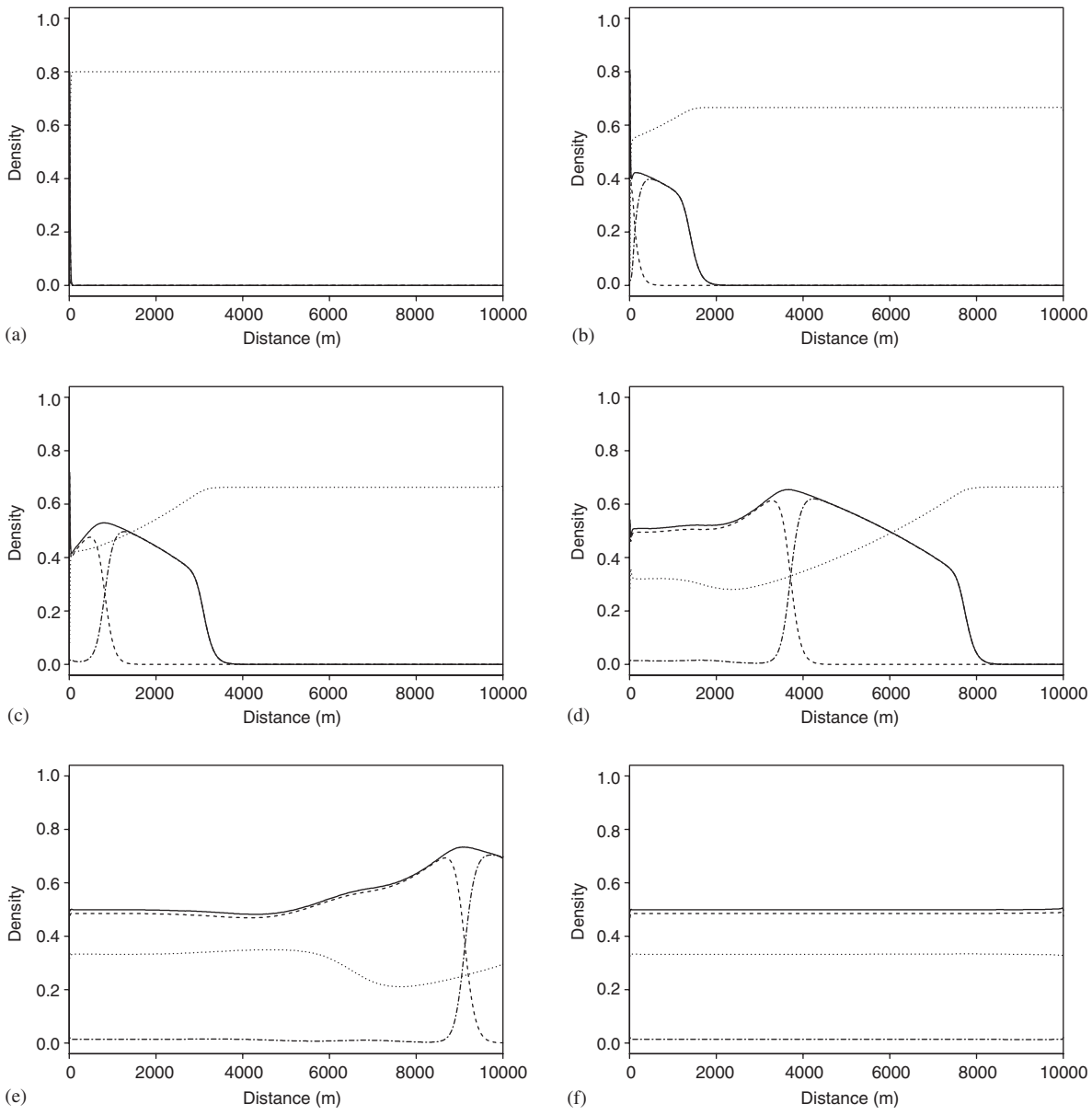

Fig. 8. Colonization dynamics in the presence of species-specific pathogens. As in Fig. 5, panels (a)–(f) show the spatial distribution of the resident (···) and colonizer (–) at different times t (years) following the arrival of the colonizing species at the edge of a one-dimensional community of the resident species at equilibrium. (a) $t = 0$ yr, (b) $t = 25$ yr, (c) $t = 40$ yr, (d) $t = 80$ yr, (e) $t = 140$ yr, (f) $t = 250$ yr. Spatial position is indicated by the distance (m) from the left edge of the domain. Also shown is the spatial distribution of the uninfected (– · – · –) and infected (– – –) proportions of the colonizing population, showing the emergence of a rapidly-moving wave of uninfected colonizers and the subsequent, slower-moving wave of the colonizer's pathogen.

where $\bar{S}_1 = \mu_1/R_0$ and $\bar{I}_1$ is given as the larger root of Eq. (B5). This is plotted in Fig. 9 (solid line).

As the figure shows, the interaction between the plants and their host-specific pathogens enables the colonizing species to enter the plant community at rates compatible with those observed in the paleo-record. While in the absence of pathogens, rates of spread were less than 5 m/yr (dashed line in Fig. 9), the colonizer now moves quickly into the community at rates in excess of 100 m/yr (solid line in Fig. 9). Note that, unlike the situation in the absence of pathogens where, when the fecundities are equal, a neutral invasion occurs and the colonizer does not increase and simply mixes into the community, rapid colonization now occurs even when the colonizer has no competitive advantage over the resident. As the competitive edge of the colonizer over the resident increases, its colonization rate in the presence of pathogens is faster still (solid line in Fig. 9).

2.3. Lag between the colonizing species and its pathogen

Another noticeable feature of the dynamics shown in Fig. 8 is the accelerating lag between the front of uninfected colonizers and the subsequent wave of infection that

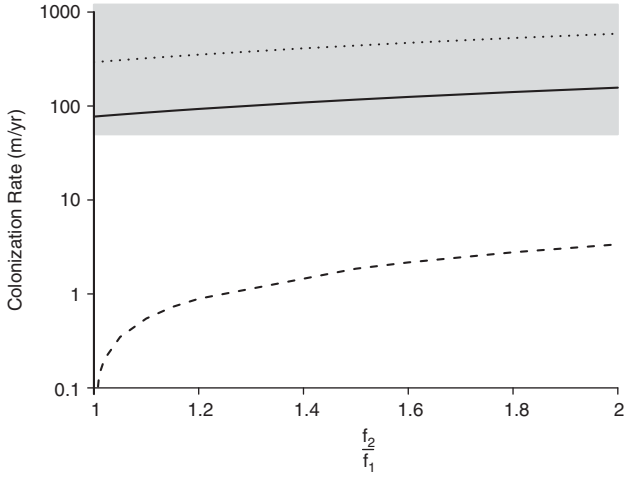

Fig. 9. Colonization rates in the absence (dashed line) and presence (solid line) of host-specific pathogens as function of the relative fecundity of the colonizing species. Plot shows the asymptotic rate of colonization c^* in m/yr as a function of f_2/f_1, the fecundity of the colonizer relative to that of the resident. Shaded area indicates the typical rates of spread observed in the paleo-record (Delacourt and Delacourt, 1987; Clark, 1998). Dashed line shows c^* for the dynamics in the absence of pathogens (Eq. (A7)). When colonizers have a fecundity advantage over the resident ($f_2/f_1 > 1$), the colonizer moves into the community with a positive characteristic asymptotic speed $c^* > 0$, but the rate of movement remains far below the typical rates observed in the paleo-record. When the species have identical fecundities ($f_2/f_1 = 1$), $c^* = 0$ and a neutral invasion occurs (see Appendix A.1). Solid line shows the rate of colonization c^* for the dynamics in the presence of pathogens (Eq. (B8)), yielding rates compatible with the rates in the paleo-record, including when the species are competitively equivalent ($f_2/f_1 = 1$). Dotted line shows colonizer's rate of movement into empty habitat (Eq. (A8)).

follows some distance behind (see Fig. 10a). This accelerating lag is perhaps surprising, since in this simulation the plants and pathogens had equal dispersal abilities (see Tables 1 and 2). This raises the question: to what extent are the rapid colonization dynamics and disruption seen in the figure dependent on the relative dispersal abilities of the plants and pathogens?

We evaluate this question further by comparing the asymptotic rate of spread of the colonizer's pathogens relative to that of the colonizing host plant population. Obtaining a full expression for the wave speed is difficult since the density of the pathogen's hosts varies spatially and temporally during colonization Fig. 8. However, as we show in Appendix B, we can derive the following equation for the rate of spread of the colonizer's pathogen c_i^*, for a given constant density, $\bar{S}_2$, of uninfected colonizing plants ahead of the infection wave:

$$c_i^* = \min_{a>0} \frac{1}{a}(R_0 \bar{S}_2 \hat{B}(a) - \mu_2). \tag{10}$$

When c_i^* is less than c^*, we expect an accelerating lag between the wave of susceptibles and infecteds. For the case of the dynamics in Fig. 8, the density of colonizing plants ahead of its pathogen S_2, is between 0.4 and 0.6 yielding a value for c_i^* of 42–85 m/yr, well below the value of $c^* = 116$ m/yr, which accounts for the observed accelerating lag (Fig. 10a).

If $c_i^* > c^*$, we might expect that the pathogens of the colonizer may enter the community at the same time as the colonizing plants. However, a more detailed analysis (Appendix B.2) suggests that this will never occur. The analysis indicates that even when the pathogen is capable of dispersing further than its host, it will enter at the rate predicted by Eq. (B8), the rate at which uninfected individuals move into a resident infected community. Moreover, the rate of increase of the pathogen at the leading edge of the wave (indicated by the eigenvalue for the infection wave) is zero, implying that even when it does colonize at the same rate as the host, it will do so at some distance behind the front of uninfected colonizers (see Appendix B.2).

Simulations of the colonization dynamics for cases where the dispersal ability of the pathogens exceed that of the plants confirm these conclusions. For example, Fig. 10b shows the dynamics of spread that arise when the plants and pathogens have the same fecundity, mortality, and infection rates as in Fig. 8, but all of the pathogen's offspring are dispersed according to the plant's long-distance dispersal kernel. In this case, the pathogens move into the community at a similar rate to the uninfected colonizers but at a fixed distance behind. Similarly, Fig. 10c shows the rates of colonization that arise when long-range dispersal capabilities of the pathogen are 10 times that of the plants. In this case, the front of pathogens accelerates toward the front of uninfected individuals but then quickly slows to the rate of spread of the uninfected colonizers. The higher dispersal ability in this case however, reduces the distance between the two fronts compared to that seen in Fig. 10b. Details of the parameter values for each of these cases can be found in Tables 1 and 2.

2.4. Effects of Niche partitioning

The model formulation explored in Sections 2.1–2.3 assumed that the two tree species contested all unoccupied sites. In this section, we generalize the community assembly model to cases where the species exhibit niche differentiation. Suppose that at each location x a fraction γ of sites are colonizable by both species, a faction γ_1 are colonizable by only species 1, and a faction γ_2 are colonizable only by species 2. $S_1(x,t)$, $S_2(x,t)$, $I_1(x,t)$, and $I_2(x,t)$ are then given by

$$\frac{\partial S_k}{\partial t}(x,t) = \underbrace{U_k(x,t) f_k \int_\Omega D(y-x)[S_k(y,t) + \delta I_k(y,t)]\,\mathrm{d}y}_{recruitment} - \underbrace{R_0^{(k)} S_k(x,t) \int_\Omega B(y-x) I_k(y,t)\,\mathrm{d}y}_{infection} - \underbrace{\mu_k S_k(x,t)}_{mortality}, \tag{11}$$

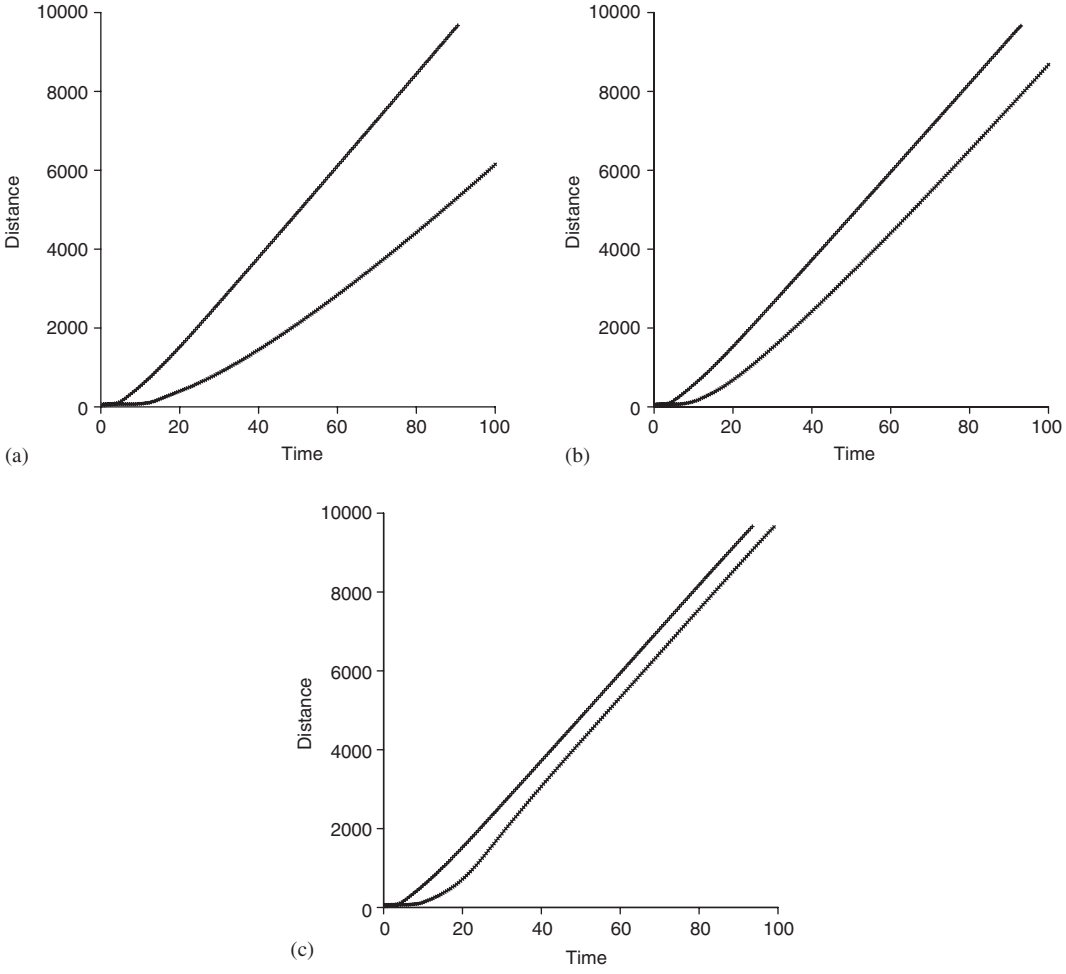

Fig. 10. (a)–(c) Distance–time plots, showing how the lag between uninfected and infected colonists varies as function of the dispersal characteristics of the pathogens. Lines show the location of the fronts of uninfected (upper) and infected (lower) individuals of the colonizing species, as a function of the time since its introduction at the left edge of the domain. Patterns of lag when (a), as in Fig. 8, the dispersal ability of the pathogens matches that of the plants, showing accelerating lag between the fronts, (b) the pathogens disperse according to the long-distance dispersal kernel of the plants, showing a constant lag between the colonizer and its pathogen, and (c), when the pathogen's dispersal ability is 10 times greater than the plant's dispersal ability. In (c), the infection front initially accelerates toward the front of uninfected individuals then slows, asymptotically matching the uninfected individuals' rate of spread. For details of the parameter values associated with each of these cases see Tables 1 and 2.

$$\frac{\partial I_k}{\partial t}(x,t) = \underbrace{R_0^{(k)} S_k(x,t) \int_\Omega B(y-x) I_k(y,t)\,\mathrm{d}y}_{\textit{infection}} - \underbrace{\mu_k I_k(x,t)}_{\textit{mortality}} \quad (k=1,2), \tag{12}$$

where $U_1(x,t)$ and $U_2(x,t)$ are given by

$$U_1(x) = K(\gamma+\gamma_1) - S_1(x,t) - \frac{\gamma}{\gamma+\gamma_2} S_2(x,t), \tag{13}$$

$$U_2(x) = K(\gamma+\gamma_2) - S_2(x,t) - \frac{\gamma}{\gamma+\gamma_1} S_1(x,t). \tag{14}$$

The above equations can be simplified by introducing the following non-dimensionalized variables:

$$S_1^* = \frac{S_1}{\gamma+\gamma_1}, \quad S_2^* = \frac{S_2}{\gamma+\gamma_2}, \quad I_1^* = \frac{I_1}{\gamma+\gamma_1}, \quad I_2^* = \frac{I_2}{\gamma+\gamma_2},$$

$$t^* = t\mu_1, \quad \mu_2^* = \frac{\mu_2}{\mu_1}, \quad x^* = \frac{x}{L},$$

$$f_1^* = \frac{f_1(\gamma+\gamma_1)}{\mu_1}, \quad f_2^* = \frac{f_2(\gamma+\gamma_2)}{\mu_1},$$

$$R_0^{(1)*} = \frac{R_0^{(1)} K(\gamma+\gamma_1)}{\mu_1}, \quad R_0^{(2)*} = \frac{R_0^{(2)} K(\gamma+\gamma_2)}{\mu_1},$$

$$\alpha_{12} = \frac{\gamma}{\gamma+\gamma_1}, \quad \alpha_{21} = \frac{\gamma}{\gamma+\gamma_2}, \tag{15}$$

where L is a characteristic length-scale from either D_1 or D_2. Inserting the above definitions into Eqs. (2)–(13), and then dropping the asterisks yields

$$\frac{\partial S_1}{\partial t}(x,t) = (1 - S_1(x,t) - \alpha_{12} S_2(x,t)) f_1 \times \int_\Omega D_1(y-x) S_1(y,t)\,\mathrm{d}y$$

$$- R_0^{(1)} S_1(x,t) \int_\Omega B(y-x) I_1(y,t)\,\mathrm{d}y - S_1(x,t), \quad (16)$$

$$\frac{\partial S_2}{\partial t}(x,t) = (1 - S_2(x,t) - \alpha_{21} S_1(x,t)) f_2 \times \int_\Omega D_2(y-x) S_2(y,t)\,\mathrm{d}y - R_0^{(2)} S_2(x,t) \int_\Omega B(y-x) I_2(y,t)\,\mathrm{d}y - \mu_2 S_2(x,t), \quad (17)$$

and

$$\frac{\partial I_1}{\partial t}(x,t) = R_0^{(1)} S_1(x,t) \int_\Omega B(y-x) I_1(y,t)\,\mathrm{d}y - I_1(x,t), \quad (18)$$

$$\frac{\partial I_2}{\partial t}(x,t) = R_0^{(2)} S_2(x,t) \int_\Omega B(y-x) I_2(y,t)\,\mathrm{d}y - \mu_2 I_2(x,t), \quad (19)$$

where the parameters α_{12} and α_{21} express the degree of niche overlap between the two species. Eqs. (7)–(8) used in our earlier analysis correspond to the case where $\alpha_{12} = \alpha_{21} = 1$.

Following procedures similar to those used to derive Eqs. (6) and (9), we can obtain the following linearized equations for the colonizer's asymptotic rate of spread c^*, in the absence and presence of host-specific pathogens:

In the absence of pathogens:

$$c^* = \min_{a>0} \frac{1}{a}(f_2(1 - \alpha_{21}\bar{S}_1)\hat{D}(a) - \mu_2). \quad (20)$$

In the presence of host-specific pathogens:

$$c^* = \min_{a>0} \frac{1}{a}(f_2(1 - \alpha_{21}(\bar{S}_1 + \bar{I}_1))\hat{D}(a) - \mu_2), \quad (21)$$

where, as before, $\bar{I}_1$ is given by the larger root of Eq. (B5). For simplicity, we consider the case where the species have similar fecundities and mortality rates (i.e. $f_1 = f_2$, $\mu_2 = 1$), the dispersal kernels of the two species are identical $B_1(x) = B_2(x)$, and niche overlap between the species is symmetric ($\alpha_{12} = \alpha_{21} = \alpha$).

Fig. 11 shows how the asymptotic invasion speed in the presence and absence of host-specific pathogens varies as a function of the degree of niche overlap between the two species. We first consider the invasion rate in the absence of host-specific pathogens (dashed line in the figure). When the two species occupy identical niches ($\alpha = 1$), since species 2 (the colonizer) has identical fecundity and mortality rates to those of the species 1 (the resident), species 2's colonization rate is zero, corresponding to the neutral invasion case identified earlier in Section 2.1. As the degree of niche similarity between the colonizer and resident, α, declines, the colonizer's asymptotic invasion rate increases linearly until, when niche similarity becomes zero ($\alpha = 0$), the colonizer's invasion rate is the same as its invasion rate in the absence of the resident. Thus, in the absence of pathogens, the impact of resident species on a colonizer's rate of spread is directly proportional to the degree of niche similarity between the two species (dashed line in Fig. 11).

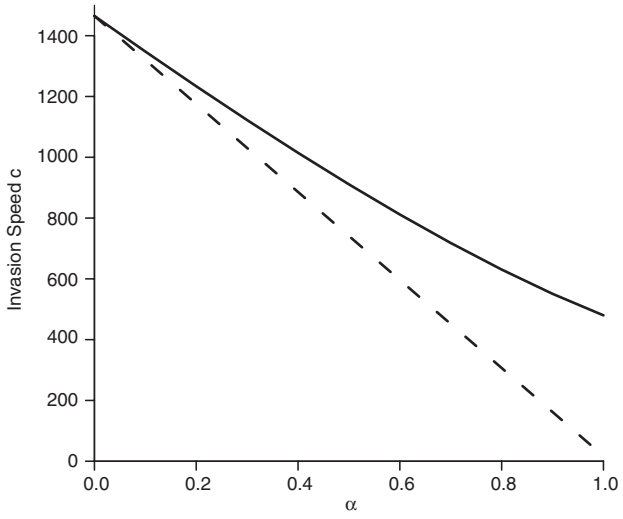

Fig. 11. Colonization rates in the presence (solid line) and absence (dashed line) of host-specific pathogens as function of the degree of niche overlap between species calculated using Eqs. (20) and (21). The effects of interactions with host-specific pathogens on a colonizer's rate of spread increases as the niche similarity between the resident and colonizer, α, increases.

In the presence of host-specific pathogens (solid line in Fig. 11), whenever the species exhibit some degree of niche similarity ($\alpha > 0$), the colonizer's rate of spread is faster than its rate of spread in the absence of the pathogens. As the figure shows, the relative difference between the colonizer's rate of spread in the presence of pathogens and its rate of spread in the absence of pathogens increases monotonically as the niche similarity between the colonizer and resident increases (solid line in Fig. 11).

3. Discussion

Recent work using single species models has shown that chance, long-range dispersal events can give rise to rates of tree migration consistent with those observed in the fossil pollen record (Clark, 1998; Higgins and Richardson, 1999). The challenge now facing ecologists and biogeographers is reconciling the rapid dynamics of spread observed in pollen studies with our knowledge of the rules and interactions that govern plant community assembly. The dynamics of multi-species communities can be complex, involving interactions that can both hinder and facilitate the spread of a particular species. However, one general principle of community theory, exemplified by detailed ecological studies of Beech and Hemlock in north-eastern forest communities (Canham, 1985; Pacala et al., 1996), is that competitively similar species will exhibit long time scales for competitive displacement.

As our analysis of a simple plant community assembly (Eqs. (1)–(2)) illustrates, when placed in the context of

patterns of tree range expansions in response to climate change, these observations of the dynamics of competitively similar species imply that Beech's rate of spread during the Holocene shown in Fig. 1 is remarkably fast given the presence of its close ecological competitor Hemlock. Thus, at least for some species, even when they have a fat-tailed dispersal kernel that enables rapid migration onto a landscape devoid of its competitors, we see a re-emergence of Reid's paradox because of the presence of ecologically similar resident species (Figs. 5 and 6).

The slowing effect of resident competitors on a colonizer's rates of spread, shown here using a model in which tree species compete mechanistically for available space and disperse according to realistic leptokurtic dispersal kernels, is consistent with the findings of Okubo et al.'s (1989) and Shigesada and Kawasaki's (1997) analyses of the phenomenological Lotka–Volterra competition equations combined with simple diffusion terms (implying Gaussian dispersal) for spatial spread. As well as confirming the robustness of their result that the reduction in the wave speed of the colonizer declines with increasing niche overlap, the analysis in Section 2.4 illustrates how colonizer's rate of spread also depends on the relative fecundities and mortality rates of the colonizer and the resident.

Our analysis suggests shows that the answer to the question of how rapid colonization can occur on landscapes occupied by ecologically-similar competitors may lie in secondary interactions with host-specific pathogens. Incorporating host-specific pathogen interactions into the simple model of plant community assembly (Sections 2.2 and 2.4), allows colonizers to rapidly migrate into landscape in which a ecologically similar species is already resident (Figs. 9 and 8). This inability of host-specific pathogens to limit the rate of spread of the colonizing host population accords with an earlier result of Owen and Lewis (2001), who found similar dynamics in a single-species, single-pathogen model.

As we have shown here, when placed into a model of plant community assembly, the ability of a colonizing species to escape its host-specific pathogens means that the colonizer temporarily behaves as a 'super-species' that outcompetes the resident species for vacant sites until its pathogens catch up. In essence, these dynamics correspond to a transient, Janzen–Connell effect (Janzen, 1970; Connell, 1971), in which a wave of uninfected colonizers reproduce and disperse ahead of their host-specific pathogen, allowing the species to migrate rapidly into the pathogen-depressed resident community.

Evidence for pathogen-induced depression of resident species comes from several studies. In particular, Davis (1981) and Allison et al. (1986) documented a rapid and widespread decline in Eastern Hemlock populations during the mid-to-late Holocene (~5400 years BP)—the signature of which is seen in the Hemlock pollen abundance maps plotted in Fig. 1a. Studies in Quebec have provided direct evidence that the mid-to-late Holocene Hemlock decline was linked to an outbreak of forest pathogens (Filion and Quinty, 1993; Bhiry and Filion, 1996).

There is also evidence that the depressing effects of resident pathogens influences subsequent rates of colonization. As seen in Fig. 1b, a rapid expansion of Beech 3000–2500 years BP occurred following the mid-to-late Holocene Hemlock decline (Davis, 1986, 1987; Woods and Davis, 1989). In addition, studies in Ontario indicate that the degree of composition change in Hemlock stands was positively associated with the extent of the Hemlock decline in the stands during the period (Fuller, 1998).

An important conclusion from the analysis in Section 2.3 is that the temporary escape from parasitism that facilitates colonizer spread is not dependent on the colonizer's pathogen having more restricted dispersal than its host. Under some circumstances, there may be an accelerating lag between the spread of a host tree species and its pathogen even when the pathogen has a greater intrinsic dispersal ability. However, the more important general result is that regardless of a pathogen's dispersal ability, its spread will lag some distance behind that of its host (Fig. 10), due to the threshold host tree density that must be exceeded in order for the pathogen population to persist. As a result, individuals at the leading edge of the colonizing population will always have a competitive edge over individuals of the resident tree species. Thus, unlike other potential mechanisms, all colonizing species will experience a period of transient competitive advantage, and hence we would not expect to see a slowing in the rates of spread of later species if they are driven by transient Janzen–Connell effects.

The effects of host-specific pathogens on tree colonization dynamics were explored here using a simple, analytically-tractable model of a plant community assembly consisting of just two ecologically-similar tree species living on a spatially and climatologically-uniform landscape. On natural landscapes, spatial heterogeneity, temporal variability and multi-species interactions will give rise to more complex patterns of spread. With regard to spatial heterogeneity, the effects of underlying abiotic heterogeneities on the performance of different species, in conjunction with the spatially-localized nature of disturbance events and tree dispersal, produces patchy spatial distributions of resident species. This, in turn, generates spatial variability in the dynamics of re-community assembly, such as that seen by Davis et al. (1994, 1998), Rejmanek (1999) and Parshall (2002) described earlier. At larger scales, gradients in climatological conditions may differentially affect the spread of colonizers and their host-specific pathogens. For example, recent evidence suggests that cold winter temperature are slowing the northward advance of the Hemlock Wooly Adelgid, a host-specific pathogen of Hemlock in the eastern United States (D. Orwig pers. comm).

With regard to temporal variability, there are two important sources of temporal fluctuations in natural communities likely to significantly affect patterns and rates

of tree colonization. First, while in the model background tree mortality rates were assumed to be constant, on actual landscapes tree mortality rates fluctuate as a result of episodic, spatially-localized disturbances. As shown here, the background rate of tree mortality is an important factor affecting the rate of colonizer spread, and thus we would expect disturbance-related fluctuations in observed rates of colonizer spread. Consistent with this prediction, several studies have found pulses in colonization rates that correlate with the occurrence of disturbance events, including fire (Eckstein, 1980; Parshall, 2002) and windthrow (Walker, 1982; Stearns, 1990; Parshall, 1995; Davis et al., 1998).

Second, many pathogens undergo episodic outbreaks. The results from this analysis suggest that fluctuations in pathogen-abundance will give rise to temporal fluctuations in the susceptibility of resident tree species to colonization, and consequently in the magnitude of the transient Janzen–Connell effect experienced by coloning species. On short time-scales, these fluctuations may arise from the nonlinear dynamics of many pathogen populations, and their sensitivity to climate variability (Moran effects). On long time-scales, co-evolutionary responses of trees to damage and mortality may give rise to long-term fluctuations in pathogen abundance and their impact on host-tree population densities. For example, the recovery of Hemlock in the late Holocene following its widespread decline 5000–4000 years BP (Fig. 1), may been the result of the evolution host resistance (Allison et al., 1986; Fuller, 1998).

While clearly idealized, the processes that give rise to the rapid rates of spread in our simple model of plant community assembly are likely to operate in similar ways in more complex models of multi-species communities living on spatially heterogeneous and climatologically variable landscapes. As we showed in Section 2.4, while niche differentiation between the colonizer and resident tends to reduce the impact of host-specific pathogens on the colonizer's rate of spread, the qualitative result that interactions with host-specific pathogens result in faster rates of migration is a general result that will hold whenever the niches of species overlap. Due to their similar resource requirements, niche overlap among tree species is generally high, particularly between species of similar successional status such as Beech and Hemlock (Fig. 2). As a result, the transient Jansen–Connell effects described here are likely to be particularly important for the post-Pleistocene range expansions of tree populations during the Holocene.

Finally, when considering tree range shifts in response to future climate change, it is important to recognize that the migrations of tree species may be quite different from those observed in the historical pollen record. In particular, the fragmented nature of modern forest landscapes and the presence of newly-introduced host-specific predators and pathogens may diminish, or further strengthen, the influence of transient Janzen–Connell effects on a species' rate of spread.

Acknowledgments

P.R. Moorcroft gratefully acknowledges funding from the Harvard University William F. Milton Fund, the Harvard University Center for the Environment, and the Harvard Forest LTER. M.A. Lewis gratefully acknowledges the support of NSERC Discovery and Collaborative Research Opportunity grants, the National Science Foundation under Grant no. DEB-0213698 and by the Canada Research Chairs program. We thank Simon Levin, Jim Clark, Helena Mueller-Landau and Michael Cain for their suggestions on the manuscript and thank Chris Preheim and Robert Bechtel for their help in preparing this manuscript for submission.

Appendix A. Rate of spread in the absence of pathogens

To calculate the invasion speed, we linearize about the leading edge of the invasion and equate the speed of the nonlinear system (Eqs. (4)–(5)) with the speed of the linearized system. Note that since this approximation is not guaranteed to work in multispecies models (e.g. Hosono, 1998; Weinberger et al., 2002; Lewis et al., 2002), we also checked our analytic wave speed calculations against numerical simulations.

If the density of the two species in front of the wave of colonizers is $S_1 = \bar{S}_1, S_2 = \bar{S}_2$ then at the leading edge of the wave we have $(S_1 - \bar{S}_1, S_2 - \bar{S}_2) = (s_1, s_2)$, where $0 \leqslant |s_1|, |s_2| \ll 1$. To leading order, the system then becomes

$$\frac{\partial s_1}{\partial t}(x,t) = \bar{U} f_1 \int_{-\infty}^{\infty} D(y-x) s_1(y,t)\,\mathrm{d}y - s_1(x,t) - f_1 \bar{S}_1 (s_1(x,t) + s_2(x,t)), \tag{A1}$$

$$\frac{\partial s_2}{\partial t}(x,t) = \bar{U} f_2 \int_{-\infty}^{\infty} D(y-x) s_2(y,t)\,\mathrm{d}y - \mu_2 s_2(x,t) - f_2 \bar{S}_2 (s_1(x,t) + s_2(x,t)), \tag{A2}$$

where $\bar{U} = 1 - \bar{S}_1 - \bar{S}_2$.

To calculate the spread rate we consider exponentially decaying traveling wave solutions of the form s_1, $s_2 \propto \exp(-a(x - ct))$. Substitution into (A1)–(A2) and application of a solvability condition yields a dispersion relation $c(a)$ between the spread rate c and the steepness of the wave a. For perturbations that are initially localized in space, we equate the spread rate of invading population c^* with the minimum speed

$$c^* = \min_{a>0} c(a). \tag{A3}$$

We need the spatially homogeneous equilibria $\bar{S}_1$ and $\bar{S}_2$ in order to evaluate the degree to which the environment is already invaded at the leading edge of the wave $\bar{U} = 1 - \bar{S}_1 - \bar{S}_2$. When species 1 has invaded previously, $\bar{S}_1 = 1 - 1/f_1$, $\bar{S}_2 = 0$ and $\bar{U} = 1/f_1$.

The case with species 2 spreading into an environment previously invaded by species 1 yields

$$\frac{\partial s_2}{\partial t}(x,t) = f_2(1-\bar{S}_1)\int_{-\infty}^{\infty} D(y-x)s_2(y,t)\,\mathrm{d}y - \mu_2 s_2(x,t). \tag{A4}$$

Substitution of an exponential decaying wave front into the above equation yields

$$acs_2 = f_2(1-\bar{S}_1)\hat{D}(a)s_2 - \mu_2 s_2, \tag{A5}$$

where $\hat{D}(a)$ is the moment generating function for the plant dispersal kernel D. Since D is a composite Laplace kernel ($D(x) = (1-p)\exp(-|x|)/2 + (1-p)\beta_l \exp(-\beta_l|x|)/2$ (see Table 1), the moment generating function is

$$\hat{D}(a) = (1-p)\frac{1}{a^2-1} + p\frac{\beta_l^2}{a^2-\beta_l^2} \tag{A6}$$

defined for a less than 1 and β_l.

Substituting (A5) into (A3) yields the following equation for the wave speed:

$$c^* = \min_{a>0}\frac{1}{a}(f_2(1-\bar{S}_1)\hat{D}(a) - \mu_2), \tag{A7}$$

where $1-\bar{S}_1 = 1/f_1$. Assuming equal mortality rates ($\mu_2 = 1$), Eq. (A7) is positive whenever f_2 exceeds f_1, indicating that colonization occurs. When there is no existing tree community, $1-\bar{S}_1 = 1$ and Eq. (A7) becomes

$$c^* = \min_{a>0}\frac{1}{a}(f_2\hat{D}(a) - \mu_2) \tag{A8}$$

Mollison's (1977) equation for the rate of spread of an epidemic.

A.1. Neutral invasion case

Assuming equal mortality rates ($\mu_2 = 1$), note that as f_2 approaches f_1 the above spread rate (A7) approaches zero. To understand this case better, we observe that when $f_2 = f_1$ Eqs. (4) and (5) add to give

$$\frac{\partial S}{\partial t}(x,t) = (1-S(x,t))f_1\int_{-\infty}^{\infty} D(y-x)S(y,t)\,\mathrm{d}y - S(x,t), \tag{A9}$$

where $S(x,t) = S_1(x,t) - S_2(x,t)$. The steady state $S = 1-1/f_1$ defines an invariant manifold for the two equation system (4) and (5): $S_1(x,t) + S_2(x,t) = 1-1/f_1$. Moreover, it is straightforward to show that this is a stable manifold, i.e., if we start close to $S_1(x,t) + S_2(x,t) = 1-1/f_1$ we will soon approach it. In the case where the resident species S_1 has density $\bar{S}_1 = 1-1/f_1$ and a few individuals of the second species S_2 are introduced locally we start close to $S_1(x,t) + S_2(x,t) = 1-1/f_1$ and approach it asymptotically. At this point the approximation $U(x,t) = 1/f_1$ is valid. Substituting this into (5) yields

$$\frac{\partial S_2}{\partial t}(x,t) = \int_{-\infty}^{\infty} D(y-x)S_2(y,t)\,\mathrm{d}y - S_2(x,t) = 0 \tag{A10}$$

and hence the invading population does not grow, but simply spreads into the resident population by redistributing spatially. A similar situation has been analysed for Lotka–Volterra competition with spread (Okubo et al., 1989; Lewis et al., 1996).

Appendix B. Rate of colonization in the presence of pathogens

Linearization of Eqs. (7)–(8) for $i = 1,2$ about the leading edge of a spreading populations leads to the following equations for perturbations about the equilibrium at the leading edge (s_1, s_2, i_1, i_2):

$$\begin{aligned}\frac{\partial s_1}{\partial t}(x,t) = {} & \bar{U}f_1\int_{-\infty}^{\infty} D(y-x)[s_1(y,t) + \delta i_1(y,t)]\,\mathrm{d}y \\ & - R_0\left(s_1(x,t)\bar{I}_1 + \bar{S}_1\int_{-\infty}^{\infty} B(y-x)i_1(y,t)\,\mathrm{d}y\right) \\ & - s_1(x,t) - f_1(\bar{S}_1 + \delta\bar{I}_1)(s_1(x,t) + s_2(x,t) \\ & + i_1(x,t) + i_2(x,t)),\end{aligned} \tag{B1}$$

$$\begin{aligned}\frac{\partial i_1}{\partial t}(x,t) = {} & R_0\left(s_1(x,t)\bar{I}_1 + \bar{S}_1\int_{-\infty}^{\infty} B(y-x)i_1(y,t)\,\mathrm{d}y\right) \\ & - i_1(x,t),\end{aligned} \tag{B2}$$

$$\begin{aligned}\frac{\partial s_2}{\partial t}(x,t) = {} & \bar{U}f_2\int_{-\infty}^{\infty} D(y-x)[s_2(y,t) + \delta i_2(y,t)]\,\mathrm{d}y \\ & - R_0\left(s_2(x,t)\bar{I}_2 + \bar{S}_2\int_{-\infty}^{\infty} B(y-x)i_2(y,t)\,\mathrm{d}y\right) \\ & - \mu_2 s_2(x,t) - f_2(\bar{S}_2 + \delta\bar{I}_2) \\ & \times(s_1(x,t) + s_2(x,t) + i_1(x,t) + i_2(x,t)),\end{aligned} \tag{B3}$$

$$\begin{aligned}\frac{\partial i_2}{\partial t}(x,t) = {} & R_0\left(s_2(x,t)\bar{I}_2 + \bar{S}_2\int_{-\infty}^{\infty} B(y-x)i_2(y,t)\right) \\ & - \mu_2 i_2(x,t).\end{aligned} \tag{B4}$$

Focusing on (B1)–(B4), we can approximate the rate of spread of the colonizing species by considering the rate at which an uninfected colonizer spreads into an infected competitor ($\bar{S}_2 = 0, \bar{I}_2 = 0, i_2 = 0$).

Plant density levels ahead of the wave are at equilibrium levels so that densities at the leading edge of the wave are $\bar{S}_1 = 1/R_0$, and $\bar{I}_1$ is given by the larger root of

$$\delta f_1\bar{I}_1^2 + \left(\frac{f_1}{R_0}(1+\delta) - \delta f_1 + 1\right)\bar{I}_1 + \frac{1}{R_0}\left(1 - f_1 + \frac{f_1}{R_0}\right) = 0, \tag{B5}$$

In this case, Eqs. (B3) and (B4) become

$$\frac{\partial s_2}{\partial t}(x,t) = (1-\bar{S}_1-\bar{I}_1)f_2\int_{-\infty}^{\infty} D(y-x) \times[s_2(y,t)+\delta i_2(y,t)]\,\mathrm{d}y - \mu_2 s_2(x,t). \quad \text{(B6)}$$

Exponentially decaying traveling wave solutions for the invader take the form $s_2 = k_1\exp(-a(x-ct))$. Substitution into Eq. (B6) yields

$$acs_2 = (1-\bar{S}_1-\bar{I}_1)f_2\hat{D}(a)s_2 - \mu_2 s_2. \quad \text{(B7)}$$

As above we compute the minimum wave speed c^* as

$$c^* = \min_{a>0}\frac{1}{a}((1-\bar{S}_1-\bar{I}_1)f_2\hat{D}(a)-\mu_2). \quad \text{(B8)}$$

As with Appendix A, our heuristic calculations given here were checked against numerical simulations.

B.1. Rate of spread of the colonizer's pathogen

We can approximate the rate of spread of the colonizer's pathogen assuming a fixed density of uninfected colonizers ahead of the wave of infection $\bar{S}_2>0, s_2=0$. In this case Eq. (B4) simplifies to

$$\frac{\partial i_2}{\partial t}(x,t) = R_0\bar{S}_2\int_{-\infty}^{\infty} B(y-x)i_2(y,t)\,\mathrm{d}y - \mu_2 i_2(x,t). \quad \text{(B9)}$$

Assuming that the threshold density of susceptibles is exceeded $\bar{S}_2 = \mu_2/R_0 > 1$ in Eq. (B9) gives us

$$c_i^* = \min_{a>0}\frac{1}{a}(R_0\bar{S}_2\hat{B}(a)-\mu_2). \quad \text{(B10)}$$

B.2. Conditions for equal rates of spread

A composite case is that of uninfected plants spreading at the speed given by Eq. (B8) followed by infected plants spreading at speed c_i^*. If $c_i^*<c^*$, then the infected plants will spread slower than uninfected plants. We conjecture that if $c_i^*>c^*$ infection will initially spread faster than the uninfected plants ahead but, as infection starts to catch up and the level of S_2 diminishes, the spread rate for infected plants will asymptotically match c^*. This will lead to a scenario where the infection follows the spreading plant population, but at a distance.

In this case $\bar{S}_1 = \mu/R_0$, $\bar{I}_1$ satisfies Eq. (B5), $\bar{S}_2 = \bar{I}_2 = 0$ and $s_2, i_2 > 0$. Eqs. (B3) and (B4) then become

$$\frac{\partial s_2}{\partial t}(x,t) = (1-\bar{S}_1-\bar{I}_1)f_2\int_{-\infty}^{\infty} D(y-x) \times[s_2(y,t)+\delta i_2(y,t)]\,\mathrm{d}y - \mu_2 s_2(x,t), \quad \text{(B11)}$$

$$\frac{\partial i_2}{\partial t}(x,t) = -\mu_2 i_2(x,t). \quad \text{(B12)}$$

Exponentially decaying traveling wave solutions for the invader take the form $s_2 = k_1\exp(-a(x-ct))$, $i_2 = k_2\exp(-a(x-ct))$. Substitution into (B11)–(B12) yields

$$acs_2 = (1-\bar{S}_1-\bar{I}_1)f_2\hat{D}(a)[s_2+\delta i_2] - \mu_2 s_2, \quad \text{(B13)}$$

$$aci_2 = -\mu_2 i_1. \quad \text{(B14)}$$

This can be rewritten as the matrix equation

$$M\begin{bmatrix} s_2 \\ i_2 \end{bmatrix} = \begin{bmatrix} 0 \\ 0 \end{bmatrix}, \quad \text{(B15)}$$

where

$$M = \begin{bmatrix} -ac + (1-\bar{S}_1-\bar{I}_1)f_2\hat{D}(a) - \mu_2 & (1-\bar{S}_1-\bar{I}_1)f_2\hat{D}(a)\delta \\ 0 & -ac-\mu_2 \end{bmatrix}. \quad \text{(B16)}$$

A non-trivial solution requires that one of the diagonal elements of M is equal to zero. If the lower right element of M is set to zero, then both upper elements are positive. The corresponding eigenvector has entries of opposite sign, and one of s_1 or i_1 is negative and hence biologically implausible. Thus, the wave speed is given by setting the top left element equal to zero so that $ac = (1-\bar{S}_1-\bar{I}_1)f_2\hat{D}(a)-\mu_2$. Proceeding as above we compute the minimum wave speed c^* as

$$c^* = \min_{a>0}\frac{1}{a}((1-\bar{S}_1-\bar{I}_1)f_2\hat{D}(a)-\mu_2), \quad \text{(B17)}$$

which is the same as Eq. (B8).

References

Allison, T.D., Moeller, R.E., Davis, M.B., 1986. Pollen in laminated sediments provides evidence for a mid-holocene forest pathogen outbreak. Ecology 67, 1101–1105.

Bhiry, N., Filion, L., 1996. Mid-holocene hemlock decline in eastern North America linked with phytophagous insect activity. Quat. Res. 45, 312–320.

Brown University Quaternary Environment Group, Bartlein, P., 2005. Pollenview v3.2. ⟨http://www.geo.brown.edu/georesearch/esh/QE/Research/VegDynam/VegAnima/PV32Inst.htm⟩.

Canham, C., 1985. Suppression and release during canopy recruitment in *Fagus grandifolia*. Bull. Torrey Bot. Club 117, 1–7.

Caspersen, J., Kobe, R., 2001. Interspecific variation in sapling mortality in relation to growth and soil moisture. Oikos 92, 160–168.

Caspersen, J., Silander, J., Canham, C., Pacala, S., 1999. Modeling the competitive dynamics and distribution of tree species along moisture gradients. In: Spatial Modeling of Forest Landscape Change, Cambridge University Press, Cambridge, pp. 14–41.

Clark, J., 1993. Paleoecological perspectives on modeling broad-scale responses to global change. In: Kareiva, P.M., Kingsolver, J.G., Hvey, R.B. (Eds.), Biotic Interactions and Global Change, Sinauer, pp. 315–332.

Clark, J.S., 1998. Why trees migrate so fast: confronting theory with dispersal biology and the paleorecord. Am. Nat. 152 (2), 204–224.

Clark, J.S., 2003. Estimating population spread: what can we forecast and how well? Ecology 84, 1979–1988.

Clark, J.S., Fastie, C., Hurtt, G., Jackson, S.T., Johnson, C., King, G.A., Lewis, M., Lynch, J., Pacala, S., Prentice, C., Schupp, E.W., Webb, T., Wycoff, P., 1998. Reid's paradox of rapid plant migration. BioScience 48(1), 13–24.

Connell, J., 1971. On the role of natural enemies in preventing competitive exclusion in some marine animals and rain forest trees. In: den Boer,

P., Gradwell, G. (Eds.), Dynamics of Populations, Wagenigen, Center for Agricultural Publishing and Documentation, The Netherlands, pp. 298–310.

Davis, M., 1976. Pleistocene biogeography of temperate deciduous forests. Geosci. Man 13, 13–26.

Davis, M. 1981. Outbreaks of forest pathogens in quaternary history. IV International Palynological Conference, vol. 3, Lucknow, pp. 216–228.

Davis, M., 1986. Dispersalversus climate: expansion of *fagus* and *tsuga* into the upper great lakes. Vegetatio 67, 93–103.

Davis, M.B., 1987. Invasion of forest communities during the holocene: beech and hemlock in the great lakes region. In: Gray, A., Crawley, J., Edwards, P. (Eds.), Colonization, Succession and Stability. Blackwell Scientific, Oxford, pp. 373–393.

Davis, M.B., Sugita, S., Calcote, R.R., Frelich, L.E., 1992. Effects of invasion by *Tsuga canadensis* on a North American forest ecosystem. In: Teller, A., Mathy, P., Jeffers, J.N.R. (Eds.), Response of Forest Ecosystems to Environmental Changes, Elsevier Applied Science, pp. 34–44.

Davis, M.B., Sugita, S., Calcote, R., Ferrari, J., Frelich, L., 1994. Historical development of alternate communities in a hemlock-hardwood forest in Northern Michigan USA. In: May, R., Webb, N., Edwards, P. (Eds.), Large-scale Ecology and Conservation Biology. Blackwell, Cambridge, MA, pp. 19–39.

Davis, M.B., Calcote, R.R., Sugita, S., Takahara, H., 1998. Patchy invasion and the origin of a hemlock-hardwoods forest mosaic. Ecology 79, 2641–2659.

Delacourt, P., Delacourt, H., 1987. Long-term Forest Dynamics of the Temperate Zone. Springer, New York.

Eckstein, R., 1980. Eastern hemlock (*Tsuga canadensis*) in north central Wiconsin, vol. 104, Wisconsin Department of Natural Resources Research Report.

Filion, L., Quinty, F., 1993. Macrofossil and tree-ring evidence for a long term forest succession and mid holocene hemlock decline. Quat. Res. 40, 89–97.

Frelich, L., Calcote, R., Davis, M., 1993. Patch formation and maintenance in an old-growth hemlock-hard-wood forest. Ecology 74, 513–527.

Fuller, J.L., 1998. Ecological impact of the mid-holocene hemlock decline in southern Ontario, Canada. Ecology 79, 2337–2351.

Higgins, S., Richardson, D., 1999. Predicting plant migration rates in a changing world: the role of long-distance dispersal. Am. Nat. 153, 464–475.

Hilker, F., Lewis, M., Seno, H., Langlais, M., Malchow, H., 2005. Pathogens can slow down or reverse invasion fronts of their hosts. Biol. Invasions 7 (5), 817–832.

Hosono, Y., 1998. The minimal speed of traveling fronts for a diffusive Lotka Volterra competition model. Bull. Math. Biol. 60, 435–448.

Huntley, B., Birks, H., Webb, T., 1988. Vegetation History. Handbook of Vegetation Science. Kluwer, Dordecht, The Netherlands.

Huntley, B., Birks, H., Webb, T., 1991. Vegetation history. Science 252, 692–695.

Janzen, D., 1970. Herbivores and the number of tree species in tropical forests. Am. Nat. 104, 501–528.

Keane, R., Crawley, M., 2002. Exotic plant invasions and the enemy release hypothesis. Trends Ecol. Evol. 17, 164–170.

Kessel, S., 1979. Adaptation and dimorphism in eastern hemlock, *Tsuga canadensis*. (l.) carr. Am. Nat. 133, 333–350.

Kot, M., Lewis, M.A., van den Driessche, P., 1996. Dispersal data and the spread of invading organisms. Ecology 77 (7), 2027–2042.

Lewis, M., Li, B., Weinberger, H.F., 2002. Spreading speed and the linear conjecture for two-species competition models. J. Math. Biol. 45, 219–233.

Lewis, M.A., Pacala, S., 2000. Modeling and analysis of stochastic invasion processes. J. Math. Biol. 387–429.

Lewis, M.A., Schmitz, G., Kareiva, P., Trevors, J.T., 1996. Models to examine containment and spread of genetically engineered microbes. Mol. Ecol. 5, 165–175.

Mitchell, C., Power, A., 2003. Release of invasive plants from fungal and viral pathogens. Nature 421, 625–627.

Mollison, D., 1977. Spatial contact models for ecological and epidemic spread. J. R. Stat. Soc. B 39 (3), 283–326.

Neubert, M.G., Kot, M., Lewis, M.A., 1995. Dispersal and pattern formation in a discrete-time predatory–prey model. Theor. Popul. Biol. 48 (1), 7–43.

North American Pollen Database Contributors, 2005. In: Grimm, E., et al. (Eds.), IGBP PAGES/World Data Center for Paleoclimatology. Boulder, Colorado: NOAA/NCDC Paleoclimatology Program.

Okubo, A., Maini, P.K., Williamson, M.H., Murray, J.D., 1989. On the spatial spread of the grey squirrel in Britain. Proc. R. Soc. Lond. B 238, 113–125.

Overpeck, J., Bartlein, P., Webb, T., 1991. Potential magnitude of future vegetation change in eastern North America: comparisons with the past. Science 252, 692–695.

Owen, M., Lewis, M., 2001. Can predation slow, stall or reverse a prey invasion? Bull. Math. Biol. 63, 655–684.

Pacala, S.W., Canham, C.D., Saponara, J., Silander, J.A., Kobe, R.K., Ribbens, E., 1996. Forest models defined by field measurements: estimation, error analysis and dynamics. Ecol. Monogr. 66, 1–43.

Parshall, T., 1995. Canopy mortality and stand-scale change in a northern hemlock-hardwood forest. Can. J. For. Res. 25, 1466–1478.

Parshall, T., 2002. Late holocene stand-scale invasion by hemlock (*Tsuga canadensis*) at its western range limit. Ecology 83, 1386–1398.

Reid, C., 1899. The Origin of the British Flora. Dulau, London.

Rejmanek, M., 1999. Holocene invasions: finally the resolution ecologists were waiting for. TREE 14, 8–10.

Shigesada, N., Kawasaki, K., 1997. Biological Invasions: Theory and Practice. Oxford University Press, Oxford.

Skellam, J.G., 1951. Random dispersal in theoretical populations. Biometrika 38, 196–218.

Stearns, F., 1990. Forest history and management in the northern midwest. In: Sweeney, J. (Ed.), Management of Dynamic Ecosystems, The Wildlife Society, pp. 107–122.

Walker, D., 1982. Vegetation's fourth dimension. New Phytol. 90, 419–429.

Webb, T., 1987. The appearance and disappearance of major vegetational assemblages: long-term vegetational dynamics in eastern North America. Vegetatio 69, 177–187.

Webb, T., Anderson, K., Bartlein, P., Webb, R., 1998. Late quaternar-yclimate change in eastern North America: a comparison of pollen-derived estimates with climate model studies. Quat. Sci. Rev. 17, 587–606.

Weinberger, H.F., Lewis, M.A., Li, B., 2002. Analysis of the linear conjecture for spread in cooperative models. J. Math. Biol. 45, 183–219.

Woods, K.D., Davis, M.B., 1989. Paleoecology of range limits: beech in the upper peninsula of Michigan. Ecology 70 (3), 681–696.